

Frozen Assets: Leveraging Ice, Water, and Phase Transitions in Robots

Aaron Wilhelm^{1*}, Andrew Wilhelm^{1*}, Lydia Isabela Calderon-Aceituno^{2*}
Nils Napp¹, Kirstin Petersen¹, and E. Farrell Helbling¹

Abstract—Robots are especially useful in cold, remote, and inhospitable environments such as polar regions and extraterrestrial settings. Due to subfreezing temperatures and limited resources in these environments, robots made of ice are particularly advantageous. In this paper we demonstrate how the solid and liquid phases of water, and transitions between these phases, can be leveraged into common robot designs for modular robots, robot arms, rovers, and soft robots. We explore how robots can utilize structural elements made of ice and exploit the phase change between ice and water to augment their capabilities. Additionally, we do a scaling analysis of ice structural elements to provide insight on their performance at different length scales and ambient temperatures.

I. INTRODUCTION

Some of the most exciting applications of robots are in subfreezing temperatures. International space agencies are targeting operation in outer space and exploration of Jupiter’s ice moon Europa [1]. Due to the increasing rate of global warming, studies of polar environments and glaciers are becoming increasingly urgent [2]. Canada is investing in winter maintenance of seasonal roads over lakes, rivers, and land to indigenous populations [3]. Weather patterns worldwide are becoming more extreme [4]. At the time of writing just three years have passed since winter storm Uri hit the United States, Northern Mexico, and Canada impacting hundreds of millions of people. It is therefore a timely contribution to study the opportunities related to robots and ice. Specifically, we investigate the use of ice and phase changes between water and ice in a range of common robot designs.

Due to their low cost and wide availability in polar regions, ice and reinforced ice have been used to build igloos (traditional, dome-shaped shelters), hotels, roads, airstrips, and even ships [5]. Ice has also been proposed for use in extraterrestrial habitats, commended for its ability to let visible light penetrate to the interior [6], [7]. However, only recently did Carroll and Yim introduce the the idea of using ice as a structural element for robots [8]. Their paper focused on low-energy manufacturing methods, comparing machining, molding, and melting, and culminated in a demonstration of two motors embedded into an ice chassis along with two ice wheels. The concept that the robot morphology may

be designed, customized, or even repaired after arrival in a subfreezing climate is promising.

The use of phase transitions (solids to liquids to gasses) to augment robot capabilities is common, especially in the soft robotics literature where it has been used to produce actuation via expansion and contraction and to tune material rigidity using a range of inorganic and organic compounds [9], [10], [11], [12], [13]. Specific to water, several research groups have also pursued the idea of freezing and melting a tip meniscus to grip micro-scale components [14], [15], [16], [17]. Here, we build on these prior advances to show additional benefits that can come from embracing the use of ice in common robot designs. Rather than considering the ice melting as a threat to structural and electronic component integrity, or the freezing of water as a risk for immobilizing the robots or breaking structural components, we utilize these phase changes to add robot capability.

In areas that can reach subfreezing temperatures, water and ice are often readily available; failed robots composed mostly of ice would have low environmental impact; and it is exceedingly easy to work with water and requires no specialized equipment. Where ice may be used as structural elements, transitioning between water and ice can lend additional benefits. Melting or fracturing ice may facilitate robot reconfiguration, foreign materials may be embedded into the ice, and the expansion of water as it freezes may be used to induce actuation forces. In this paper, we first perform a scaling analysis of the structural strength and melting characteristics of ice. In subsequent sections we then explore different capabilities of ice in simple robotic systems and demonstrate these concepts across a range of classic robot morphologies including modular robots, robot arms, rovers, and soft robots.

II. SCALING ANALYSIS OF ICE STRUCTURAL ELEMENTS

Due to its low cost and relative strength, an obvious use for ice on a robot is as a structural element. Past work by Carroll and Yim [8] use ice for a rover chassis, and in our experiments we use ice rods as structural elements for a modular robot and a robotic arm. To provide better intuition, we reason about the structural integrity and melting of ice at different length scales and ambient temperatures. For our derivations, we assume a set aspect ratio between r (rod radius, 10 mm) and L (rod length, 73 mm) and scale them each by a factor β_s , but our work can be expanded to other ice rod aspect ratios.

*The first three authors contributed equally to this work.

¹School of Electrical and Computer Engineering, Cornell University, Ithaca, NY 14853, USA. ajw344@cornell.edu, ajw343@cornell.edu, nnapp@cornell.edu, kirstin@cornell.edu, farrell@cornell.edu ²Sibley School of Mechanical and Aerospace Engineering, Cornell University, Ithaca, NY 14853, USA. lic27@cornell.edu

A. Stress Constraint

Ice is a brittle material, so structural failure of the rod at large scales is caused by high tensile stress. The stress in a cylindrical member due to a uniformly distributed load can be primarily considered as bending stress, given by:

$$\sigma = \frac{My}{I},$$

where σ is the bending stress, M is the bending moment, y is the distance from the rod's neutral axis to the point where the stress is to be calculated, and I is the moment of inertia of the cross-section about the neutral axis.

For a simply supported rod with a uniformly distributed load, the bending moment is $M = \frac{\omega}{2}(x(L-x))$, where ω is mass per unit length, x is distance from one end of the rod, and L is the rod's total length.

The effects of scaling on relevant variables are:

- Length terms (x , y , L , and r) scale linearly with β_s
- Moment of inertia I' scales as $I' = \beta_s^4 I$
- Mass scales by β_s^3 , and is incorporated into ω , which scales by β_s^2 since it represents mass per unit length
- Bending moment M scales with ω multiplied by length squared, which gives $M' = \beta_s^4 M$

The total effect of scaling on the bending stress is

$$\sigma' = \frac{(\beta_s^4 M)(\beta_s y)}{\beta_s^4 I} = \beta_s \sigma$$

Therefore, stress on the rod will increase linearly with the scaling factor β_s and will fail once it reaches the average tensile strength of ice $\sigma_t = 1.9 \text{ MPa}$ [18]. The maximum scaling before failure is $\beta_{\max} = \frac{\sigma_t}{\sigma_0}$.

B. Melting Constraint

When using ice as a building material, one also needs to consider the effects of melting. Because of the large surface area along the length of the rod, we assume that the ice rod's radius will melt significantly faster than its length, increasing the stress experienced by the rod and leading to structural failure. We denote this time as the critical time and in the following work we identify minimum values of β_s that guarantee a minimum critical time until failure.

We first calculate the melting rate of the rod's radius. The heat required to melt ice is given by $Q = mL_f$, where m is the mass of the ice and L_f is the latent heat of fusion for ice. The rate of heat transfer can be approximated using Newton's law of cooling, which is $\dot{Q} = hA\Delta T$, where h is the heat transfer coefficient, which accounts for properties of the ambient air surrounding the rod, A is the area of the rod, and ΔT is the difference between the ambient temperature and the temperature of the rod. It follows that $\dot{m} = \frac{\dot{Q}}{L_f}$, which can be related to change in volume \dot{V} via density of ice ρ , $\dot{V} = \frac{d}{dt}(\pi r^2 L) = \frac{\dot{Q}}{\rho L_f}$. This yields

$$\dot{r} = \frac{\dot{Q}}{(2\pi r L)\rho L_f} = \frac{h(2\pi r L)\Delta T}{(2\pi r L)\rho L_f} = \frac{h\Delta T}{\rho L_f} \quad (1)$$

under the assumption that melting only reduces the radius.

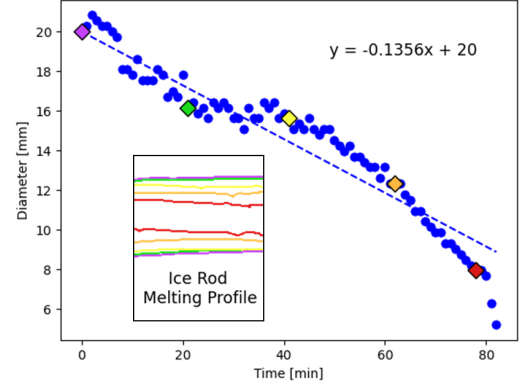


Fig. 1. Recorded profile and radius of an ice rod in room temperature. The outline as the rod melts is illustrated under the graph, with the respective time frame of each outline indicated by its color.

As the rod melts, the tensile strength it undergoes increases until it reaches σ_t , at which point it fractures. The time it takes for this to occur is its critical time. In order for the rod to not fail due to melting, a length scale with a critical time greater than the desired time of operation must be selected.

To verify that our model accurately reflects the melting rate \dot{r} , we performed a melting test and calculated the average melting rate of an ice rod (made from tap water). The ice rod was secured on one end, and its width measured every minute until it fractured under its own weight due to melting. A plot of the rod diameter over time can be seen in Fig. 1. Overall, the ice rod melts evenly around the circumference of the rod and the average melting rate was found to be 0.1356 mm/min. Calculating Eq. 1 with the experimental ambient conditions resulted in a theoretical melting rate of 0.1221 mm/min which is a 10% error from the observed value.

C. Scaling analysis

The effect of temperature on the melting constraint can be seen in Fig. 2. Intuitively, the minimum allowable length scale increases with temperature and desired minimum critical time.

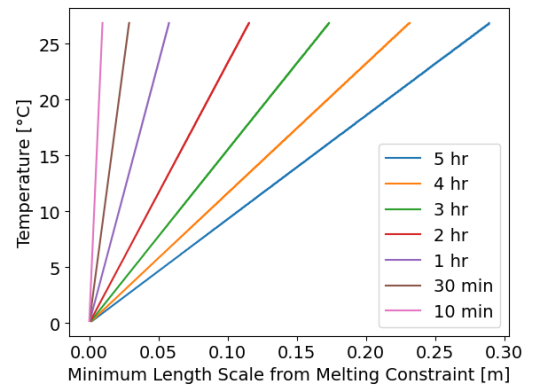


Fig. 2. Smallest possible length scales, subject to the melting constraint, for different operating temperatures and desired minimal critical times.

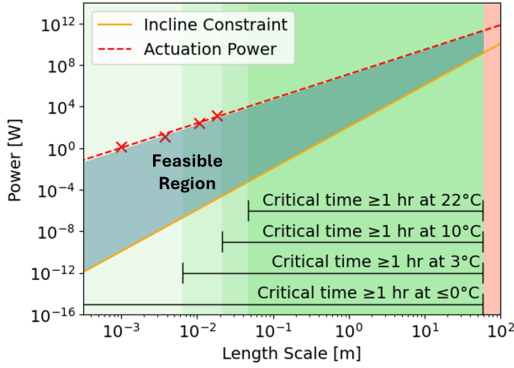


Fig. 3. Feasible region of operation for a robot with a structural ice rod like the one used in Sec. III at different length scales. At large length scales, the rod exceeds the tensile strength of ice (red region) and at small length scales, the ice rod melts before achieving a critical time ≥ 1 hr at different ambient temperatures (green shaded regions). The feasible region is also bounded by robot design constraints (orange line) and the approximate maximum actuation power for the corresponding length scale (dashed red line fitted using specifications from commercially available DC motors, indicated as red crosses).

When designing an ice robot, a roboticist must ensure that at a given length scale, the ice structural members satisfy the melting and stress constraints while still meeting the standard set of design constraints typically found in traditional (non-ice) robots. Fig. 3 illustrates some of the considerations that must be made when designing robots composed of ice rods at different length scales and environmental temperatures. Length scales that are infeasible for ice robots due to the rod stress constraint (Sec. II-A) are found in the red shaded region, and length scales in which ice robots can have a critical time longer than one hour before melting at various temperatures (as discussed in Sec. II-B) are found within the corresponding green shaded regions. Design constraints, traditionally found in (non-ice) robots (e.g., the minimum power required to move an ice robot up an incline and the maximum actuator power¹), provide bounds on the feasible region. These design constraints are application specific. In our example, we have chosen an incline of 5° and a minimum velocity of 1 BL/s. Less stringent constraints would increase the size of the feasible region. Of course, robots may have different rod cross-sections, load profiles, and more than one rod, but this analysis gives an initial intuition for the design considerations of ice robots.

III. MELTING STRUCTURAL ICE ELEMENTS

One of the advantages of using ice as a structural element in robot design is that it can be melted to change the robot's structure. This is especially useful for a modular rover, which is composed of many segments, each capable of independent operation, but collectively capable of aggregate motion, better terrain maneuvering, and greater

¹DC motor specifications collected from (pololu.com) and (mcmaster.com)

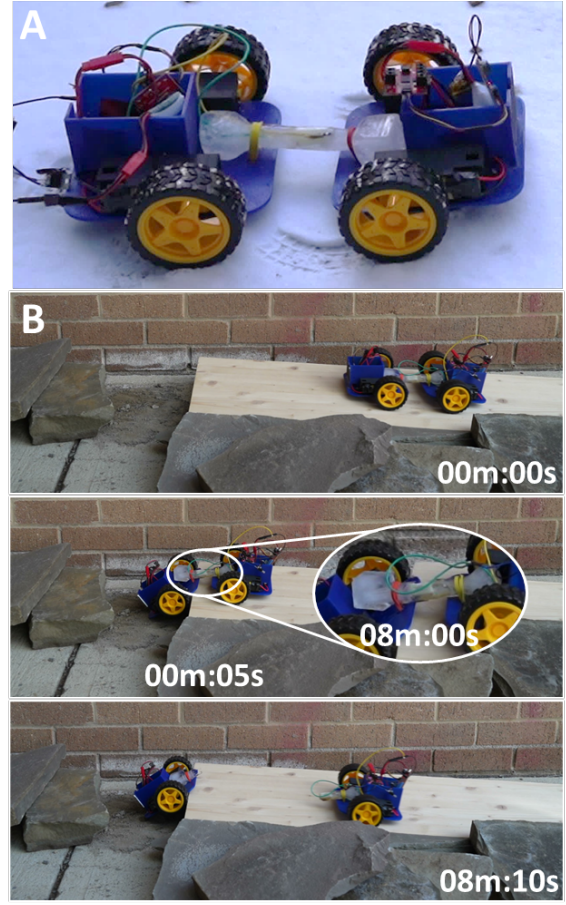


Fig. 4. A) Modular robot composed of two differential drive modules connected together with an ice rod. B) Upon encountering an environmental hazard that prevents the rover from navigating, the rover thermally melts the ice rod using a high power resistor, and the rear module drives away.

payloads [19]. A particular benefit of such a design is the ability to shed faulty or entrapped segments when needed. In this section, we demonstrate how a modular rover can melt its ice coupling to shed a module that has become entrapped in an environmental hazard.

To show the core principle of reconfiguration upon encountering environmental hazards, we designed and built two modules (Fig. 4A). Each module included a 3D printed chassis onto which we mounted two 120:1 plastic gear motors with a 90° shaft and two wheels, an Artemis Nano board controllable via Bluetooth, a DRV8833 dual motor driver board, and a single-cell 850 mAh Li-Po battery.

We molded a 73 mm long ice rod, 20 mm radius, using local tap water and connected each end to a module using rubber bands, which maintain holding force if the rod melts. Before freezing, we embedded a waterproofed $5\ \Omega$, 5 W power resistor within the mold. Then we connected a MOSFET driver circuit on the rear module to the resistor, powering it by a separate single-cell 850 mAh Li-Po battery, i.e. consuming roughly 2.74 W.

We then operated the robot in -3°C and drove it over a ramp, upon which it became stuck (Fig. 4B). To recover, the

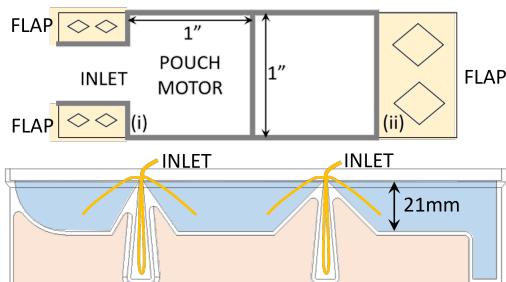


Fig. 5. Design of 3-link robot finger. The top sketch shows the pouch motor design from a single consecutive sheet: gray surfaces were laminated together, first by the inlet and middle, then seal (ii) was welded onto seal (i) to produce a pouch motor with two flaps marked in yellow. The bottom sketch shows a cross-sectional view of the finger mold. Compartments for frozen water are shown in blue; compartments for hot water to release the cast is shown in red. Two pouch motors, shown in yellow, were frozen into the links to double as flexible joints.

robot melted the connection between the modules thereby freeing the back module. It took 8 min to melt the rod to a point at which the back module was able to induce a fracture and drive off. This ability to reconfigure during run-time may be helpful during exploration of difficult-to-navigate environments.

IV. FRACTURING STRUCTURAL ICE ELEMENTS

In addition to melting, ice elements can be fractured for robot reconfiguration. We designed a 2-DOF robot finger in which the 3 links were made of ice roughly $50 \text{ mm} \times 21 \text{ mm} \times 25 \text{ mm}$ in length, width, and height respectively. To actuate the finger, we embedded pouch motors [20] in each joint, such that inflation would stretch the finger, and deflation aided by gravity would curl the finger.

We fabricated two $1 \times 1 \text{ in}^2$ pouch motors (Fig. 5 top), consisting of 2 mil polyethylene tubing from U-Line. A single pouch motor design can be seen in Fig. 5. Gray lines, representing seals, were laminated together with a heat sealer. First, we patterned a single inlet sized to accommodate a flexible silicone tube and a thin silicone collar. We used a zip tie around the inlet to create an airtight seal. We then patterned the tubing to create the desired shape. Flaps made of excess tubing material were encased in the ice as the water solidified. These flaps were covered in Gaffers tape and small holes were cut to enable additional water penetration. We then placed two pouch motors into a mold as shown in Fig. 5 bottom. The mold was filled with water and placed

in a freezer. Once solidified, the finger was demolded, and a syringe was attached to each pouch motor.

These experiments were performed at room temperature. As seen in Fig. 6A, each pouch motor expanded up to 8 mm, causing a change in angle between link 1 and 2 by 7° , and a change of 15° between link 2 and 3. The pouch motor design also resulted in a working flexible joint, although as the ice melted, the slack between the fingers grew larger.

Figure 6B shows a second finger, composed of just the two outer links. Two pouch motors were laminated together. The first actuated the joint, as described above, and the second was embedded in the outermost link, replacing the perforated flap. Both pouches were coupled to a single syringe, and when inflated at low pressure, the finger repeatedly bent (Fig. 6Bi-ii), showing stable operation. When inflated at high pressure, the embedded pouch motor caused a fracture (Fig. 6Biii), and the entire link was shed off of the robot. This ability may be useful to help robots abandon parts which are stuck or otherwise broken in the field.

V. ICE/WATER PHASE CHANGES TO ADAPT ROBOT COMPONENTS

The phase change between water and ice can also be exploited to expand the capability of a robot. To showcase this benefit, we designed a rover that has wheels cast from ice. Utilizing melting and freezing cycles, the rover can reconfigure its wheels as needed when navigating an environment.

The rover was composed of a custom 3D printed chassis, with 120:1 plastic gear motors with a 90° output shaft, controlled by an Artemis Nano board and a DRV8833 dual motor driver, and powered by a single-cell 400 mAh Li-Po battery and a 700 mAh NiCd battery. We designed custom 3D printed hubs (Fig. 7A, inset), inspired loosely by those designed in [8] and froze these directly into ice wheels, which were molded into a cylindrical mold with a 80 mm diameter and a depth of 20 mm.

The first experiment is shown in Fig. 7B. We drove the rover up to a tunnel that was too small for it to fit into. The rover then used common sidewalk salt to chemically melt 25 mm off the wheel diameter, driving over the salt continuously to ensure even distribution of the salt over the circumference of the wheels. The experiment was conducted outside in -3°C . Melting the wheels took ~ 20 min. Additionally, the robot can also utilize existing heat sources in the environment. We showcased this by conducting an experiment where a heated metal plate heated was used



Fig. 6. A) 3-link robot finger, composed of ice links and 2 pouch motors which also serve as flexible joints to hold the links together. B) 2-link robot finger, shedding its outer link by over-inflating the corresponding pouch motor to produce an ice fracture.

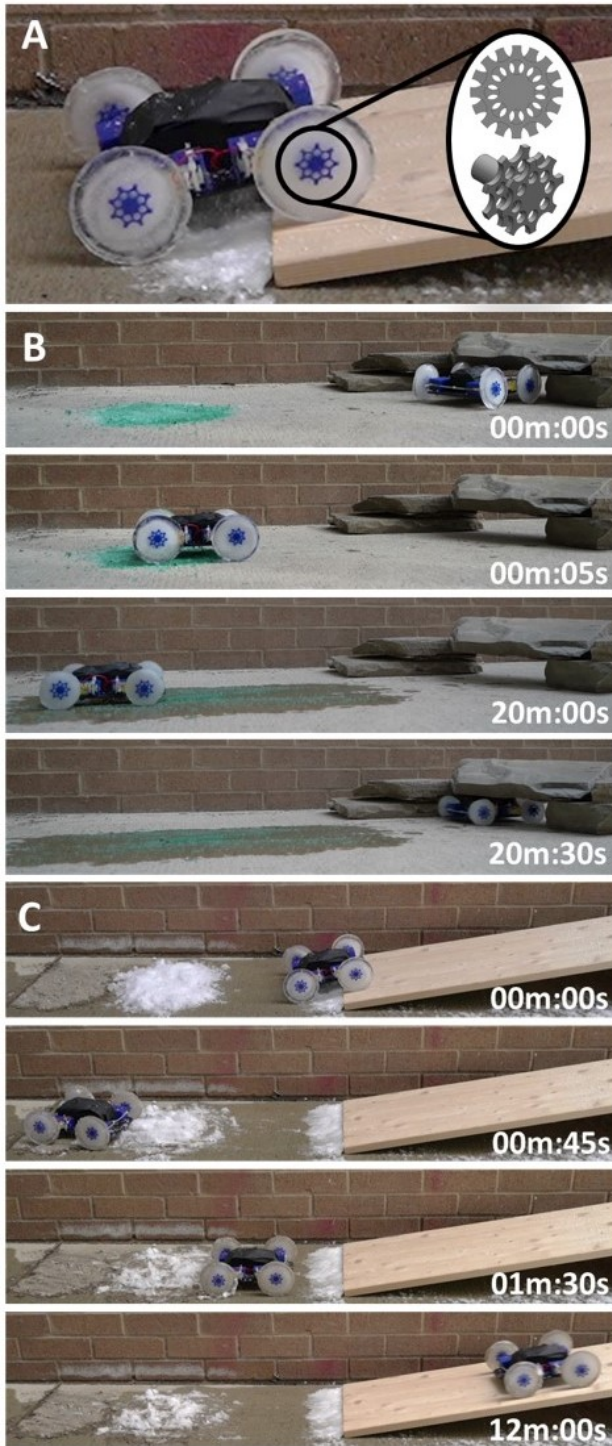


Fig. 7. A) Rover with ice wheels molded around 3D printed wheel hubs. B) Rover utilizing salt to chemically melt its ice wheels to fit under a low clearance obstacle. C) Rover with two ice wheels attempting to climb a 9.4° incline. Upon failing, the rover embeds and freezes sand into its wheels and is now able to ascend the slope.

to melt the wheels. The robot first melts its front wheels and then its back wheels on the hot plate, melting 10 mm off of each set in ~ 8 min total. For both experiments, we found it important to continually spin the wheels to ensure

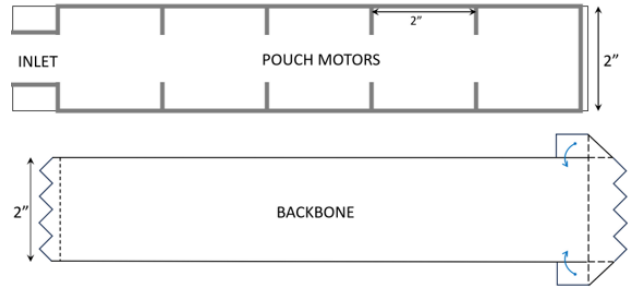


Fig. 8. The inchworm is composed of pouch motors and a flexible backbone. The pouch motors were laminated as shown along the gray bars. The backbone was made from 10 mil acrylic sheets, and folded 90° along the long dashed lines and $\sim 120^\circ$ along the short dashed lines. The pouches and backbone were attached using 0.25" strips of Gaffers tape.

even melting and keep the circular shape. When using a heating element, we observed significantly slower melting rates if water was allowed to pool on the hot surface. To account for this, we found it beneficial to have the heating element at a slight angle so the water could run off. For these experiments, a sufficient wheel diameter was determined via observation; however, the robot could perform this with on-board sensing (e.g., using a distance sensor to measure the clearance between the chassis and the ground).

The third experiment is shown in Fig. 7C. Here, the rover tried to drive up a ramp with a 9.4° incline in subfreezing temperatures, but the wheels slipped due to the low friction between the ice and ramp. The robot then drove over snow and a layer of construction sand composed of particles with an average diameter of 0.25–4 mm. The crystalline structure of snowflakes creates a film of liquid water on their surface [21]. Thus, driving the ice wheels first through snow facilitates the adhesion of sand and pebbles. Once its wheels are covered, the rover stops moving to let the sand completely freeze to the wheels (10.5 min). Afterwards, the rover was capable of driving up the incline. This ability to absorb environmental materials may prove useful to overcome diverse surfaces during exploration.

VI. ICE/WATER PHASE CHANGES TO INCREASE PAYLOAD CAPACITY

In addition to structural elements, water and ice can play a key role in actuation and payload capacity in soft robots. We fabricated three inchworm robots composed of five 2×2 in² pouch motors in series, with a single inlet in the back. The pouch motors were taped loosely with Gaffers tape to a flexible backbone composed of 10 mil thick acrylic bent into back and front feet (Fig. 8). For lack of snow, the experiments were performed on a Styrofoam surface.

The results from one of three trials are shown in Fig. 9. We inflated the inchworm by injecting ~ 40 mL water, then repeatedly added and removed an additional 40 mL to produce forward motion. In its relaxed state, the inchworm lays flat on the ground due to both the elastic tension of the backbone, and the baseline weight of the water in the pouch motors. When water is added, the pressure in the pouch

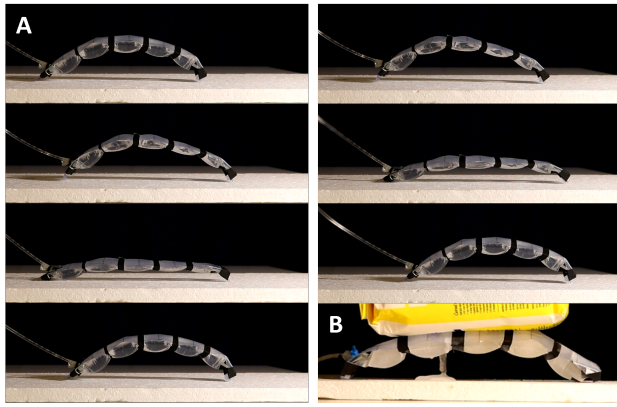


Fig. 9. A) Two steps by a 5-chamber pouch motor inchworm robot. B) Frozen inchworm holding a 1.88 kg payload.

motors causes contraction and, like a tendon, they produce a bending strain on the backbone. The inchworm traveled an average of $28 \text{ mm/step} \pm 16 \text{ mm}$ or 10.8% (lay-flat) body lengths per step.

While water can successfully actuate the inchworm to cause forward motion, it was only capable of sustaining small perturbations on the backbone without foot displacement. However, once frozen, the inchworm could hold a 1.88 kg mass with no noticeable deflection (Fig. 9B). The expanding water caused a small leak resulting in the thin pillar of ice in the image. In applications, water-based robots could be deployed, move to a desired position, and then serve as a structural element once frozen.

Finally, the expansion of water when it freezes (up to 110%) can actuate hydraulic robots. We assembled two 3-chamber pouch motors similar in design to the the inchworm, and filled them with 45 mL of water, leaving some room for expansion. We then hung two weights, 206 g and 483 g, respectively, and measured their length before and after freezing. Before freezing, the pouch motor length was measured to 130 mm and 135 mm, due to the different gravitational forces from the weights. Upon freezing, the pouch motors both contracted to roughly 120 mm, indicating that the expansion force provided by water easily overcomes the maximum load. We were limited by the height of the available freezer, but presumably with more pouch motors and therefore a larger water volume, this difference could be amplified.

VII. SUMMARY

In this paper we provide a theoretical basis to suggest length scale regions where the operation of ice robots is feasible. Furthermore, we demonstrate that the use of ice, and in particular transitions between water and ice, has many potential benefits for robots with applications in rovers, wheels, robot arms, and inchworms. As water and ice are abundant in the polar regions and can change phase relatively easily, they are an attractive and versatile method of actuation and transformation in rigid and soft robots.

VIII. ACKNOWLEDGEMENT

This work was funded by a Packard Fellowship for Science and Engineering and NSF grants #2042411, #1846340, #2054744, and DGE#2139899.

REFERENCES

- [1] M. Lattimore, R. Karban, M. P. Gomez, E. Bovre, and G. E. Reeves, "A model-based approach for Europa lander mission concept exploration," in *2022 IEEE Aerospace Conference (AERO)*. IEEE, 2022, pp. 1–13.
- [2] C. Strawhacker, "Meeting the opportunities and challenges of the navigating the arctic program at the national science foundation," in *AGU Fall Meeting Abstracts*, vol. 2019, 2019, pp. PA54A–01.
- [3] K. Koch, "Nordicity and its relevance for northern Canadian infrastructure development," *Polar Geography*, vol. 44, no. 4, pp. 255–281, 2021.
- [4] J. E. Walsh, T. J. Ballinger, E. S. Euskirchen, E. Hanna, J. Mård, J. E. Overland, H. Tangen, and T. Vihma, "Extreme weather and climate events in northern areas: A review," *Earth-Science Reviews*, vol. 209, p. 103324, 2020.
- [5] N. Vasiliev, A. Pronk, I. Shatalina, F. Janssen, and R. Houben, "A review on the development of reinforced ice for use as a building material in cold regions," *Cold Regions Science and Technology*, vol. 115, pp. 56–63, 2015.
- [6] M. Morris, C. Ciardullo, K. Lents, J. Montes, O. Rudakevych, M. Sono, Y. Sono, and M. Yashar, "Mars ice house: using the physics of phase change in 3d printing a habitat with h₂o," in *Aiaa Space 2016*, 2016, p. 5528.
- [7] N. Vasiliev, A. Pronk, I. Shatalina, F. Janssen, and R. Houben, "A review on the development of reinforced ice for use as a building material in cold regions," *Cold Regions Science and Technology*, vol. 115, pp. 56–63, 2015.
- [8] D. Carroll and M. Yim, "Robots made from ice: an analysis of manufacturing techniques," in *2020 IEEE/RSJ International Conference on Intelligent Robots and Systems (IROS)*. IEEE, 2020, pp. 1933–1938.
- [9] L. Wang, Y. Yang, Y. Chen, C. Majidi, F. Iida, E. Askounis, and Q. Pei, "Controllable and reversible tuning of material rigidity for robot applications," *Materials Today*, vol. 21, no. 5, pp. 563–576, 2018.
- [10] H. Ma, X. Xiao, X. Zhang, and K. Liu, "Recent advances for phase-transition materials for actuators," *Journal of Applied Physics*, vol. 128, no. 10, 2020.
- [11] R. Chellattoan, A. Yudhanto, and G. Lubineau, "Low-voltage-driven large-amplitude soft actuators based on phase transition," *Soft robotics*, vol. 7, no. 6, pp. 688–699, 2020.
- [12] X. Li, H. Duan, P. Lv, and X. Yi, "Soft actuators based on liquid–vapor phase change composites," *Soft Robotics*, vol. 8, no. 3, pp. 251–261, 2021.
- [13] S. M. Mirvakili, D. Sim, I. W. Hunter, and R. Langer, "Actuation of untethered pneumatic artificial muscles and soft robots using magnetically induced liquid-to-gas phase transitions," *Science Robotics*, vol. 5, no. 41, p. eaaz4239, 2020.
- [14] D. Lukman, R. Šafarič, and G. Škorc, "Development of microgripper system," in *2011 XXIII International Symposium on Information, Communication and Automation Technologies*. IEEE, 2011, pp. 1–7.
- [15] D. Lang, M. Tichem, and F. Warner, "An industrial prototype of a liquid solidification based micro-gripping system," in *2007 IEEE International Symposium on Assembly and Manufacturing*. IEEE, 2007, pp. 227–232.
- [16] Y. Yang, J. Liu, and Y.-X. Zhou, "A convective cooling enabled freeze tweezer for manipulating micro-scale objects," *Journal of Micromechanics and Microengineering*, vol. 18, no. 9, p. 095008, 2008.
- [17] S. Uran, R. Šafarič, and B. Bratina, "Reliable and accurate release of micro-sized objects with a gripper that uses the capillary-force method," *Micromachines*, vol. 8, no. 6, p. 182, 2017.
- [18] J. Petrovic, "Review mechanical properties of ice and snow," *Journal of Materials Science*, vol. 38, pp. 1–6, 2003.
- [19] A. Brunete, A. Ranganath, S. Segovia, J. P. De Frutos, M. Hernando, and E. Gambao, "Current trends in reconfigurable modular robots design," *International Journal of Advanced Robotic Systems*, vol. 14, no. 3, p. 1729881417710457, 2017.
- [20] R. Niiyama, X. Sun, C. Sung, B. An, D. Rus, and S. Kim, "Pouch motors: Printable soft actuators integrated with computational design," *Soft Robotics*, vol. 2, no. 2, pp. 59–70, 2015.
- [21] C. Hosler and R. Hallgren, "The aggregation of small ice crystals," *Discussions of the Faraday Society*, vol. 30, pp. 200–207, 1960.